Delft University of Technology

A recovery system for the key components of the first stage of a heavy launch vehicle

Dek, Casper; Overkamp, Jean Luc; Toeter, Akke; Hoppenbrouwer, Tom; Slimmens, Jasper; van Zijl, Job; Areso Rossi, Pietro; Machado, Ricardo; Hereijgers, Sjef; Kilic, Veli

Important note
To cite this publication, please use the final published version (if applicable).
Please check the document version above.

Contents lists available at ScienceDirect

Aerospace Science and Technology

www.elsevier.com/locate/aescte

A recovery system for the key components of the first stage of a heavy launch vehicle ☆

Casper Dek, Jean-Luc Overkamp, Akke Toeter, Tom Hoppenbrouwer, Jasper Slimmens,
Job van Zijl, Pietro Areso Rossi, Ricardo Machado, Sjef Hereijgers, Veli Kilic, Marc Naeije *

TU Delft, Faculty of Aerospace Engineering, Kluyverweg 1, 2629HS Delft, the Netherlands

A R T I C L E   I N F O

A B S T R A C T

In recent years, the space market has been pushing towards decreasing costs of launching spacecraft by reusing parts of the launchers. The purpose of this article is to present a feasibility study of a recovery system for the engine and engine frame of an existing, expendable heavy launch vehicle and present recommendations for further research.

The concept developed is verified based on the Ariane 6. The recovery of the *Vulcan Aft Bay (VuAB)* is initialised by separation from the first stage at 157.7 km altitude while travelling at 6930 m/s. The study investigates an inflatable aeroshell for protection and deceleration during re-entry, after which it is proposed to further decelerate the VuAB using drogue parachutes. The final part of the concept entails retrieval of the VuAB by a helicopter in mid-air. To enable a controlled gliding flight during retrieval a parafoil is proposed. At launch, the recovery system will weigh 2789 kg with a payload penalty of 720 kg. The system can be integrated into the existing design of the launcher and will not interfere with nominal operations of the launcher. Implementing the recovery system can reduce the cost per launch of an Ariane 6 by 15%

1. Introduction

In recent years the market for space launch vehicles has seen significant change. Private companies have been increasingly innovative, pushing towards significant cost reductions and increased economies of scale. As of recently, especially re-usability has been of great interest. Lower stages of launchers, due to the relatively low separation from the launcher, are the first hurdle to take.

To assess the potential of recovery, a technology review has been conducted to evaluate the potential of new recovery system methods. The most promising concepts from this review are utilised as part of a feasibility study to investigate the possibility of integrating these innovative recovery system elements in an existing launcher design. The goal is to induce low payload penalties, low redesign investment requirements and achieve a decrease in cost over a launch campaign of several launches in order to enable existing launchers to be partly reusable.

This paper provides a trade-off of promising new technology from the technology review, followed by a feasibility study of the most promising concept. The mission profile is discussed, followed by a description of the different phases of flight and recovery. Finally, the integration of the recovery system and the launcher is discussed, leading up to a discussion on the feasibility of the first stage heavy launch vehicle recovery system, followed by the conclusion and future recommendations.

This paper is based on the thesis report of 10 Bachelor Aerospace students at Delft University of Technology (TU Delft). The research has been conducted using the Ariane 6 launcher as a basis. Technical data for this purely academic exercise was provided by TU Delft, through cooperation with Airbus Defence and Space Netherlands (the 'client'). The Ariane 6 first stage was chosen, since its high separation velocity and altitude would make this a challenging engineering exercise. Inquiry into the full report can be made to the corresponding author.

2. Methodology

The overall methodology and steps taken in this research are presented in this section. For this research, several recovery concepts have been generated and analysed on a top-level manner. The concepts were generated based on similar research and ex-

isting solutions for recovery methods of objects from space and high-altitude flight. After concept generation, these concepts were analysed in a comparative manner, using both quantitative and qualitative measures. The quantitative measures include the induced weight of the total system, as well as the induced payload penalty of this extra weight. The sizing of the systems for this analysis was performed using similar methods as introduced in later sections of this article. Also, the estimated development and per-item cost of the concept were taken into account. Qualitative measures include the ability of the concept to safely return the object to Earth, development time and development risks and the integration possibilities in existing launchers. For the last three of these, the goal in mind was to be able to launch the newly designed system on an existing launcher within 5 years time.

Based on this trade-off a concept was chosen, which was then further analysed. This analysis was performed by first identifying the full mission profile to be executed by the recovery system. Based on this mission profile, the sizing of all components of the recovery system was performed. The sizing of the components and determining the overall mission profile was an iterative process considering that the weight of the components has a direct relation to the velocities and distances covered in all mission phases and vice-versa. The methods used to perform the sizing of the components and to assess the overall feasibility of the concept are introduced in separate sections accompanied by the results and outcomes of these methods.

3. Concept generation and trade-off

The mission of the recovery system is to recover the engine bay of the first stage of the Ariane 6 and to allow it to be refurbished and reused for subsequent launches. Recovery shall start after separation of the first stage at 157.7 km altitude above the Atlantic Ocean, travelling at 6930 m/s velocity [18,6]. Following a literature study and evaluation of comparable missions, multiple concepts have been developed. Using design option tree logic, feasible options are selected. These design options are then compared in a trade-off that evaluated the *Technology Readiness Level (TRL)*, the mission risk, the predicted payload penalty, the costs, and the development risk of each concept.

For comparison, the currently best performing and feasible reusable systems from the aerospace sector are the reusable booster stages employed by SpaceX on their Falcon 9 and Falcon Heavy launchers [2]. SpaceX operates a fully reusable first stage on their Falcon 9 and Falcon Heavy launchers, which are steered and decelerated through a combination of thrust from the reignited and gimballed engines and control from grid fins. Additionally, Airbus Defence and Space proposed a concept, Adeline, that featured fixed wings, actuated control surfaces and electric engines, mounted on the engine bay [1]. This will allow for a conventional fixed wing landing on a runway, either on land or on a boat. Furthermore, two concepts utilising a combination of an inflatable heat shield and an autonomous guided parafoil have been evaluated. The first performs a soft landing in a large boat-mounted net, while the second is retrieved through a *Mid-Air Recovery (MAR)* using a helicopter.

In the trade-off, the concept similar to Adeline has been discarded due to a disproportional high development risk as their design will interfere with the existing launcher design. Additionally, the high envisioned costs and high payload penalty make this infeasible. Similarly, a SpaceX-type vertical thrust powered landing has been discarded. This is because the significantly larger velocity and altitude of the Ariane 6 at the first stage separation in comparison to the Falcon 9 means either excessive amounts of propellant for deceleration before re-entry are required or a re-design of the mission profile is needed. The analysed concepts and reasons for

Table 1

Analysed concepts and reasons for rejection.

Concept	Main reason for concept rejection
Horizontal fixed wing landing	Large interference with design and operations of existing launchers
Vertical thrust-powered landing	High separation altitude and speed, resulting in large amount of propellant and high induced payload penalty
Parafoil - net landing	Highly sensitive to errors in landing position
Mid-air recovery	– (selected concept)
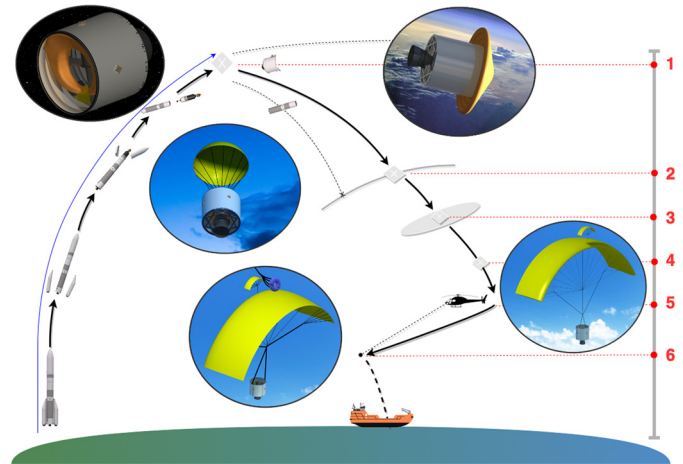
Fig. 1. Mission profile for the mid-air recovery concept.

Table 2

Mission profile details as visualized in Fig. 1, 'Distance' is ground distance with respect to separation.

Mission event	Alt. [km]	Time [s]	Distance [km]
1. Separation	157.7	0	–
2. Re-Entry	100	240	1634
3. Drogue parachute deployment	8.1	724	2844
4. Parafoil deployment	7.3	734	2844
5. Start alignment phase	4	1248	2854
6. Start catch window	1.2	1759	2852

rejection can be found in Table 1. A controlled landing in a boat-mounted net was discarded due to the slow manoeuvrability of boats large enough for such a catch. Finally, a MAR concept was selected, owing to its relatively low mass and the ability to integrate the system with minimum redesign of the original launcher.

4. Mission profile

With the MAR concept selected for the feasibility study, the mission profile is determined and visualized in Fig. 1. Table 2 gives the details about the different mission phases. The Ariane 6 is scheduled to launch from Guiana Space Center. After liftoff, first and second stage separation is performed. With no flown trajectories available from the Ariane 6, data on the Ariane 5 is used for the separation altitude and accompanying launcher velocity, as the Ariane 6 is expected to have a similar trajectory. The separation altitude and launcher velocity are fixed at 157.7 km and 6930 m/s respectively [6]. This was confirmed by our contact at Airbus Defence and Space Netherlands (2018). Until this point, nothing is changed from the original launch sequence of the Ariane 6 in order not to interfere with normal operations. Next, the VuAB separation from the first stage occurs. An inflatable aeroshell will deploy in
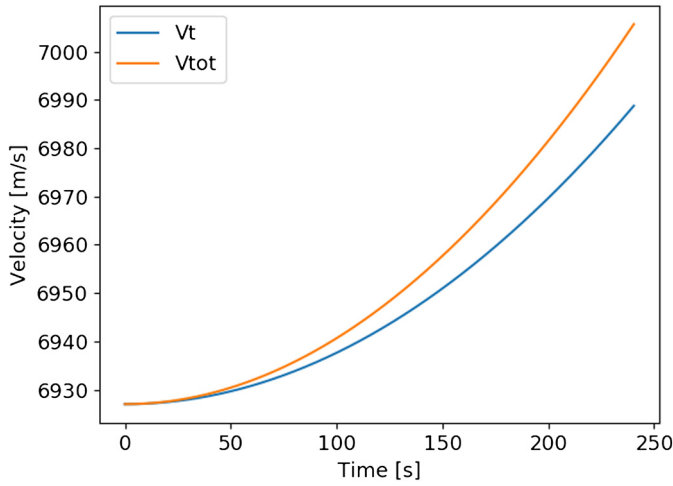
Fig. 2. Velocity of the VUAB after the space flight phase.

Fig. 3. Predicted Space Flight Phase Trajectory of the VUAB.

space, followed by atmospheric re-entry at a velocity of 7005 m/s and flight path angle of -20°. At 8 km altitude and a VuAB velocity of 85 m/s a drogue parachute deploys, followed by parafoil deployment at 27 m/s. This occurs at an altitude of 7.3 km and depicts the start of the guided parafoil descent. This parafoil ensures a horizontal and vertical flight velocity of 18 m/s and 4.5 m/s, respectively. From 4 km altitude onward, the parafoil and helicopter will begin alignment procedures. At 1.2 km the catching phase commences and the parafoil velocities are 15 m/s and 3.9 m/s horizontal and vertical respectively. In Fig. 7 it is shown that these velocities allow for a helicopter to recover the VuAB in mid-air. After the VuAB is recovered, it is landed on a recovery vessel which ships the VuAB to France in order for it to be refurbished and reused.

5. Space flight phase

The mission of the VuAB recovery system commences with the separation of the VuAB from the first stage. This separation is performed with pyrotechnics and induces rotational motion on the VuAB [18]. This rotational motion needs to be damped, in order to position the VuAB for re-entry.

The space flight phase starts at 157.7 km altitude, ends at 100 km altitude and its duration is approximated at 4 minutes using a trajectory calculation. For this purpose, a space flight model is developed that models and simulates a ballistic trajectory with an *Attitude Determination and Control System (ADCS)* for attitude control. In this model, the angular momentum per unit mass, H, is used, which is constant throughout the space flight phase and determined using Equation (1):

$$H = V_t \cdot R_e = V \cdot (R_e + h) \tag{1}$$

where V_t is the tangential velocity, R_e is the radius of the Earth and h is the altitude of the VuAB, which is defined as 100 km at the point of re-entry [22]. Using this equation, the velocities at the end of the space flight phase we determined, as shown in Fig. 2. The shape of the ballistic trajectory is defined using Equation (2):

$$p = \frac{H^2}{\mu} \tag{2}$$

assuming an elliptical shape of the trajectory and p being the semi-latus rectum defining that shape, with μ being the standard gravitational parameter for Earth. The final space flight trajectory is predicted to be as depicted in Fig. 3.
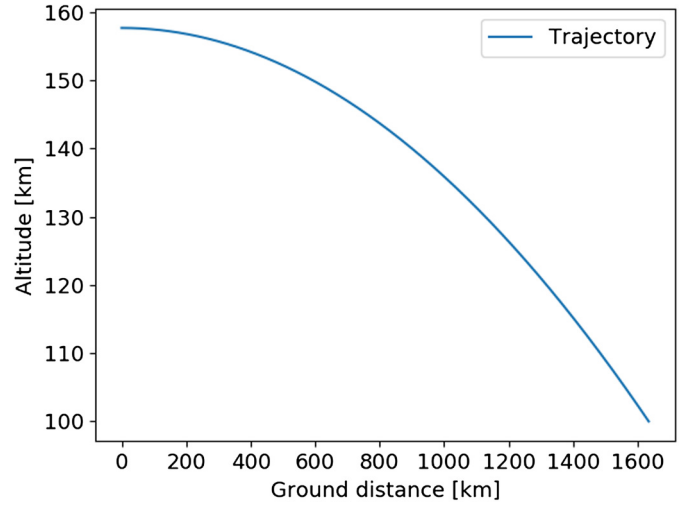
The model is able to pinpoint the re-entry location given initial separation conditions as stated in the mission profile. A controller is used to ensure the VuAB is in the desirable orientation at the start of the re-entry mission phase, and makes pitch adjustments when required. This allows the attitude control thrusters, including the required propellant, to be sized. Based on a maximum space flight time of 4 minutes and a slew rate of 8.6 deg/s at separation [18], the DST-13 thruster by MOOG [28] is selected. With a thrust of 22 N and a specific impulse of 300 s, the required propellant mass to fuel the 16 thrusters, four thrusters at each of the four sides, is computed at 0.7 kg.

6. Re-entry

At 100 km altitude, travelling at 7005 m/s, the atmospheric effects become non-negligible. The high velocity at re-entry results in high dynamic pressures and high heat flux, such that a *Thermal Protection System (TPS)* is required to protect the VuAB from these aero-thermal loads. Due to the limited amount of volume on the VuAB a rigid aeroshell cannot be integrated, so therefore an inflatable aeroshell is designed for this purpose. This aeroshell is based on existing designs by NASA, namely the HEART [10] and IRVE-III [8] concepts.
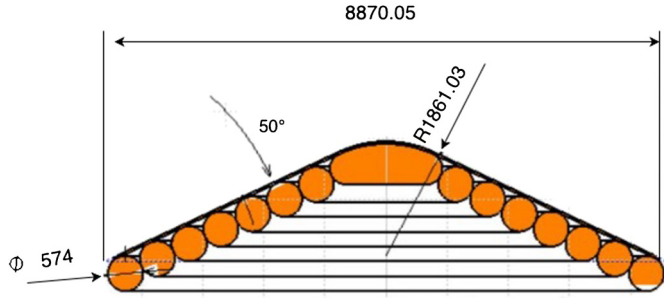
A gliding re-entry model is developed to simulate the re-entry trajectory and conditions. The re-entry model uses a linearised gravity model for a spherical Earth, with the International Standard Atmosphere (ISA) and consists of a linearisation of the $C_D - Mach$ relation of [26] for $M > 2$ for an initial angle of attack $\alpha = -20°$. The stability of the VuAB during re-entry with deployed aeroshell is analysed by comparison with the aeroshell in [19], which is stable at $\alpha = -20°$. To include small variations in the angle of attack in the reentry model, the relation between C_D and α of [19] is linearised around $\alpha = -20°$. The initial conditions of the re-entry are taken from the end of the space flight phase and integrated to size the aeroshell in an iterative process. First the nose cone diameter D_i, aeroshell diameter D_0, spherical-cone angle θ, nose-radius R_{nose}, toroid diameter D_t and number of stacked toroids N, are sized and determined using Equation (3) [25,24,21]:

$$D_t = \frac{D_o - D_i}{(2N - 1)\sin(\theta_a) + 1 - \cos(\theta_a)} \tag{3}$$

with an initial value of $N = 7$ in the first iteration. Furthermore, D_0 is constrained to a minimum diameter of 9.14 m to prevent interference of the incoming flow with the VuAB under an angle of attack of $\alpha = -20°$. Subsequently, the heatflux and dynamic pressure

Table 3

Aeroshell component mass breakdown.

Components	%	Mass [kg]
Adapter	22.1	311.4
Heatshield support stucture	5.1	71.9
Inflation mechanism	16.8	236.7
Separation mechanism	12.4	174.7
TPS	43.6	614.3
Total	100	1409

Fig. 4. Cross-section view of the aeroshell components.

Fig. 5. Verification of the re-entry model using the same design parameters used for the High-Energy Atmospheric Re-entry Test [10].

Fig. 6. Measurements performed during the High-Energy Atmospheric Re-entry Test [10].

are determined for laminar compressible flow, using Equation (4) and (5) [4]:

$$\dot{q}_w = \sqrt{\rho_\infty} V_\infty^3 \left(\frac{1.83 \cdot 10^{-8}}{\sqrt{R_{nose}}} \right) \left(1 - \frac{h_w}{h_0} \right) \tag{4}$$

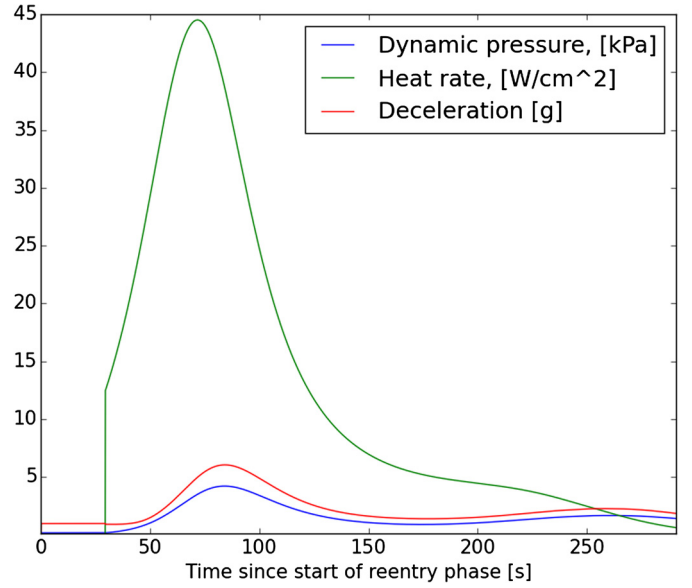$$q_\infty = \frac{1}{2} \gamma \, p_s M_\infty^2 \tag{5}$$

in which h_w is the enthalpy at the wall, h_0 is the total enthalpy, ρ_∞ is the free stream density, V_∞ is the velocity, p_s is the static pressure and M_∞ is the free stream Mach number. Since the aeroshell can be considered a blunt body, the maximum heat flux is assumed to occur at the stagnation point of the aeroshell [4]. The maximum heatflux and maximum dynamic pressure are used to select the TPS material. This yields a conservative TPS material selection since the heatflux will be lower than the maximum heatflux outside the stagnation point. Next, N, D_0, θ, R_{nose}, D_t and the selected TPS material properties are substituted in a mass model based on a modified lifting HIAD mass model [33], which results in Table 3.

The final aeroshell design has a diameter of 8.8 m, uses the ablative SIRCA-flex as the TPS material and has a mass of 1409 kg. Fig. 4 shows the cross-section of the aeroshell in its inflated state, clearly showing the inflatable toroid structure. The aeroshell is designed to fit into the engine bay by means of deflation of the toroids and subsequent folding of the deflated structure, as can be seen in the cross-section in Fig. 13, in which the beige-coloured structure represents the folded and packaged aeroshell.
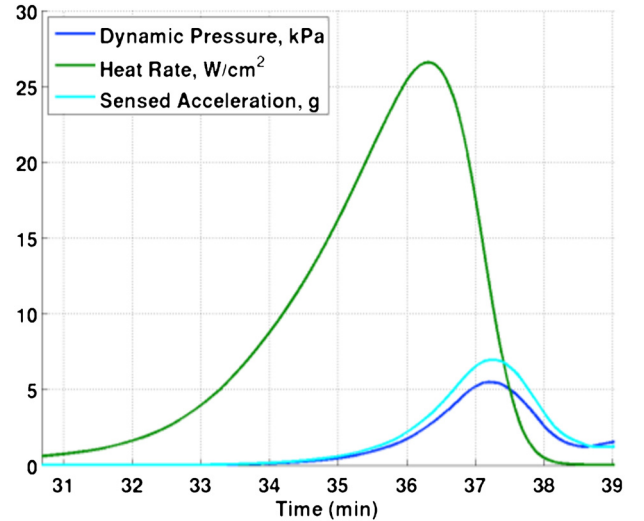
In order to verify the outputs of the developed reentry model, the same design parameters as the HEART aeroshell are used as an input to the model, after which the outputs, plotted in Fig. 5 are compared with the measurements performed during the HEART test as displayed in Fig. 6 [10].

As can be seen when comparing Fig. 5 with Fig. 6, the magnitude of the outputs is comparable. The difference between maximum heat rate found at the surface is likely due to a difference in aeroshell geometry such as the nose-cone radius. The phenomenon of higher dynamic pressure and acceleration for the HEART is likely caused by a higher kinetic energy at the start of the atmospheric entry, as this test is being performed after separation of the International Space Station.

In the next 500 seconds, the aeroshell decelerates the VuAB to around 85 m/s, covering a ground distance of 1200 km. A simula-

tion of the vertical re-entry trajectory is performed using the sizing data from the aeroshell, varying atmospheric data and the varying aerodynamic parameters throughout re-entry. The aerodynamic parameters of the aeroshell are estimated using relationships between angle of attack, mach number and the aerodynamic lift, moment and drag coefficients, as defined by [26] and [19]. The results of this simulation can be seen in Fig. 7 and Fig. 8.

In reality, atmospheric conditions are stochastic, hence a Monte Carlo simulation of the re-entry flight phase is performed to evaluate the accuracy of a re-entry using an aeroshell. This is done by varying atmospheric conditions and flight parameters such as angle of attack and the aerodynamic coefficients over a span of 1000 simulations, which can be seen in Fig. 9. The variation in the inputs during this Monte Carlo simulation are given in Table 4. The deceleration is shown in Fig. 10, showing a maximum deceleration of a little over 6 g at around 100 s corresponding to an altitude of 60 km (Fig. 7).

The accuracy of the recovery strongly depends on atmospheric conditions and external forces and is strongly influenced by slight
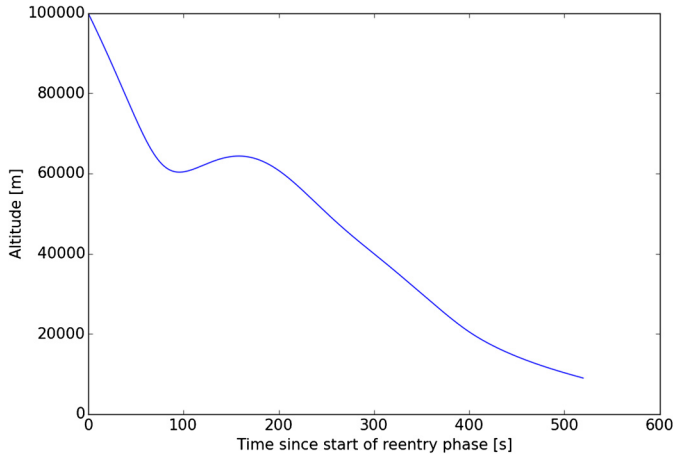
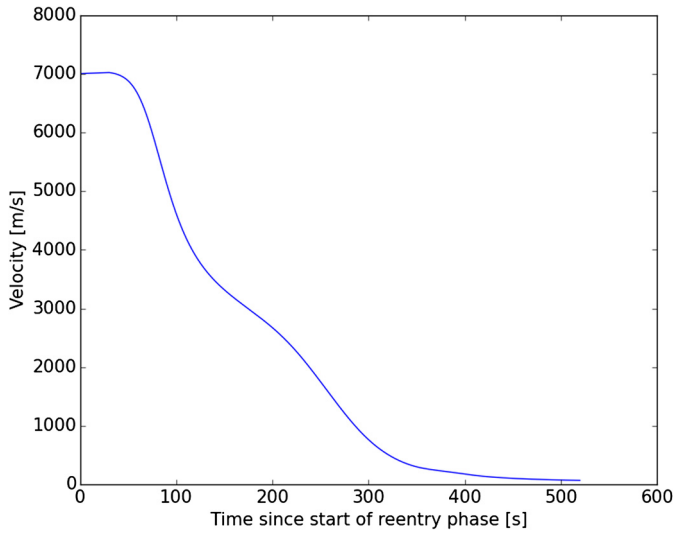**Fig. 7.** Altitude of the VuAB versus time during the re-entry phase.

Fig. 8. Velocity versus time of the VuAB during the re-entry phase.
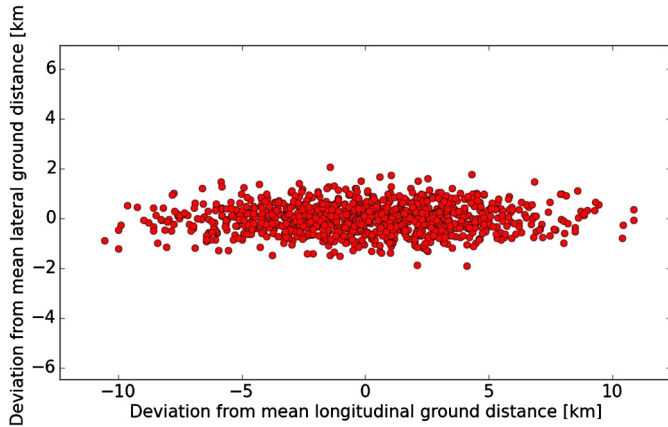

Fig. 9. Scatterplot of the Monte Carlo Simulations.

delays in separation. However, the Monte Carlo simulations do indicate that upon variation of atmospheric conditions, aeroshell surface area and angle of attack, the VuAB would not end its re-entry phase outside of the range of the retrieval helicopter. In the worst case scenario, the re-entry phase of the VuAB ended 15 km from the expected location (see Fig. 9), which means that the retrieval helicopter would still be capable of reaching it within the duration of the atmospheric flight phase.

Table 4
Uncertainties as used in the Monte Carlo Simulation.

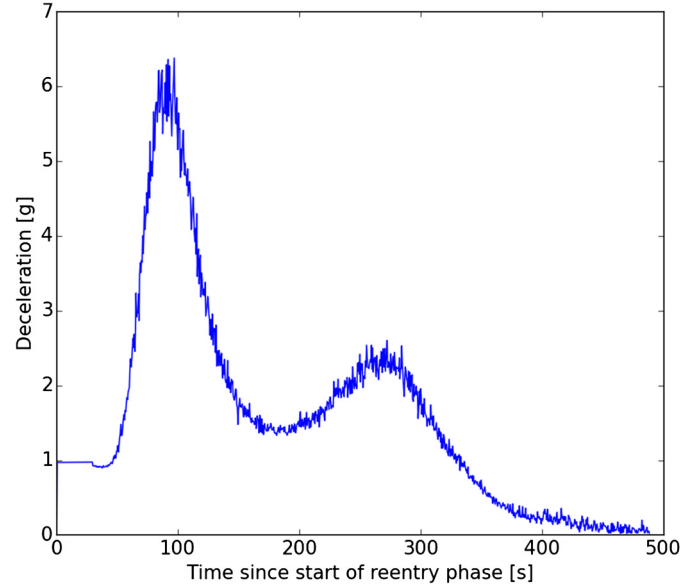| Variable	Random deviation (2σ)
Aeroshell surface area	2%
Air temperature	5%
Air pressure	5%
Air density	5%
Angle of attack	2.7 deg
Sideslip angle	2.7 deg

Fig. 10. Deceleration of the VuAB versus time for one of the atmospheric entry simulations performed during the Monte Carlo analysis.

The atmospheric entry distribution shows a predicted range of potential locations at which the atmospheric flight phase starts, the size of this distribution is 26 km longitudinally and 4 km laterally. This range of uncertainty in the re-entry position serves as an input to the required parafoil performance and control system sizing.

The aeroshell must be discarded before drogue parachute deployment. Due to volume and temperature constraints, the parachute and aeroshell deployment direction is oriented opposite to the nozzle. Therefore the VuAB needs to be flipped 180 degrees along the lateral axis before parachute deployment. This discarding and rotation is performed by gradual deflation of the aeroshell which causes a pitch up moment that rotates the VuAB, allowing the aeroshell discarded by means of a spring mechanism.

7. Atmospheric flight and recovery

In order to transition from the re-entry phase to the atmospheric flight phase, a drogue parachute is sized which is able to decelerate the VuAB further. This drogue parachute uses a forced ejection by means of a mortar, which is sized at 26 kg by means of a comparative study into mortars for parachute deployment [16]. The parachute and parafoil deployment system is constrained by a maximum allowed deceleration of 4.5 g [18], and a descent velocity below 5 m/s to provide the helicopter with sufficient time to reach and capture the VuAB. This provides the limits in which the parachute has to operate. The parachute is sized using the assumptions that the VuAB will experience a 2 second delay between discarding the aeroshell and parachute deployment, resulting in a free-fall. Also, during deployment the VuAB is assumed to move in near-vertical direction and the drag coefficient is assumed to be similar to the parachutes of the Orion [3]. The parachute sys-
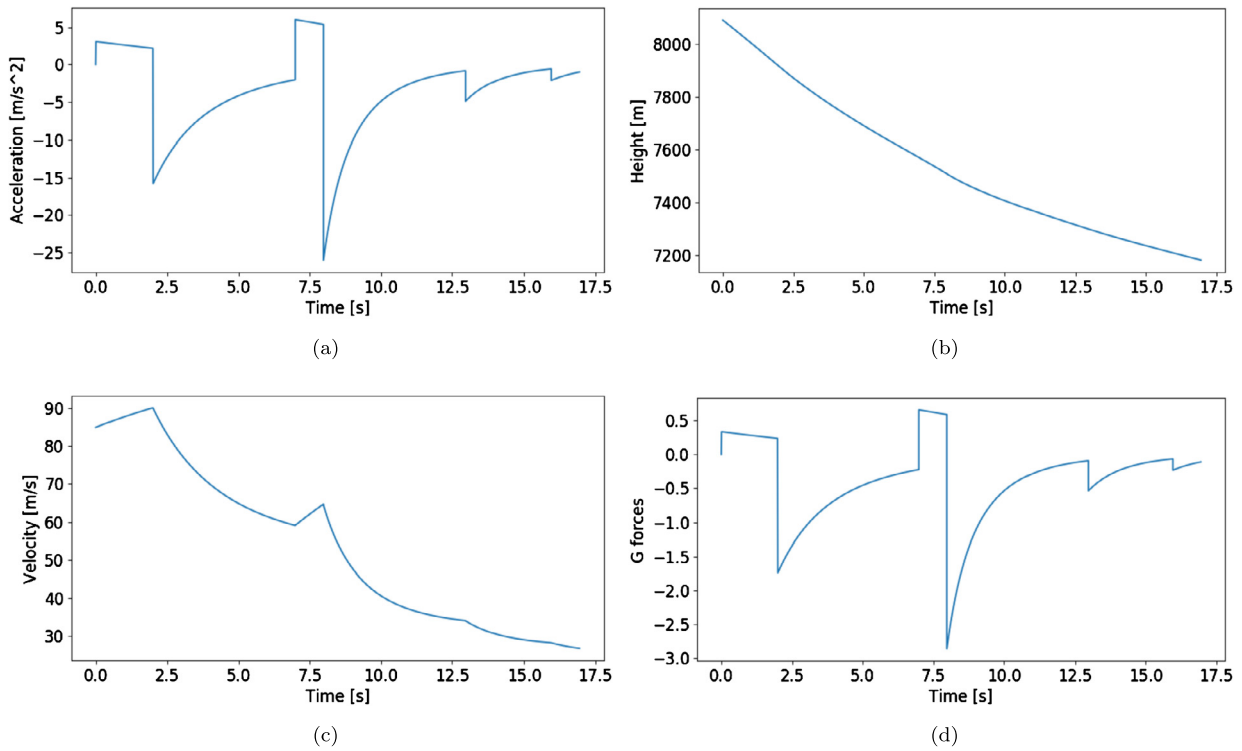
(a)

(b)

(c)

(d)

Fig. 11. The acceleration, altitude, velocity and g-forces throughout the deployment phase of the drogue parachute and parafoil.

Table 5
Parachute system masses and their respective volumes.

System	Mass [kg]	Volume [kg/m^3]
Drogue parachute	47.00	0.065
Main parafoil	435.5	0.604
Secondary parafoil	75.67	0.105
Mortar	26.00	0.036
Control system	32.66	0.045
Margin	123.4	0.171
Total	740.1	1.028

tem was designed and sized using the Orion mission as a reference [15] and using a model consisting of simple lift and drag equations as a first approximation. The mass and packing volume of all components of the system can be seen in Table 5.

The drogue parachute decelerates the VuAB to a velocity of 27 m/s at an altitude of 7.3 km, allowing the parafoil to be released and extracted by the parachute. The parachute is detached from the parafoil, after which the parafoil is inflated by gradually disreefing individual sections using a ram air system [30]. The accelerations and velocities during this process can be seen in Fig. 11. The first peak deceleration at 2 seconds coincides with the deployment of the drogue parachute at 8.1 km altitude. The second peak occurs between 7 and 8 seconds and is the result of parafoil deployment. The parafoil design and sizing is inspired by the Megafly system developed by Airborne Systems [13]. The surface area of the parafoil is sized to 836 m^2, using the desired maximum descent velocity and again a model of simple lift and drag equations as a first approximation.

A six degree of freedom, twelve state atmospheric flight model is developed to simulate the dynamic behaviour of the parafoil in flight and to aid in the design of the guidance systems based on [27,30,7,31]. This model uses three degrees of freedom for position and three for orientation. The latter three use Euler angles which contain singularities at certain orientations. It is assumed the parafoil will fly mostly straight and level based on flight her-

itage data [5]. Therefore use of Euler angles in the model is considered acceptable.

The parafoil is controlled using an *Air Guidance Unit (AGU)*, which contains the control system hardware and two servos that control two elevons at the trailing edge with a span of 20.7 m and chord of 3.5 m each. The elevons can either be deployed symmetrically to act as brake, or asymmetrically to turn the parafoil. The maximum turn performance of the control system is limited to 5 degrees per second, to prevent heavy oscillations which occur whenever this turn rate is exceeded.

The AGU does not require any inner control loops as the parafoil is designed to be inherently stable. Oscillations are present, but verification using models of [31] showed these do not pose a problem for safety or performance. Therefore, the AGU only has a heading control function, which it performs using two different modes: a trajectory mode and an energy management mode. The trajectory mode steers the parafoil towards the pick-up point, immediately after parafoil deployment. The trajectory mode controls the parafoil using a *Proportional and Differential (PD)* controller that controls the desired heading of the parafoil by means of elevon deflections. The differential control is required to damp out the oscillations that are a result of wind gusts as well as the payload suspended below the parafoil acting as a pendulum in turning maneuvers. The energy management mode is used when the VuAB is at the pick-up point to loiter in a square pattern above the retrieval location to prepare for the MAR, which is between 4 and 1.2 km altitude.

At an altitude of 4 km, the pre-catch phase begins, when the helicopter starts to align in front of the VuAB. The Sikorsky CH-53K King Stallion is selected as a suitable helicopter for the mission. It has a payload carrying capability of 14500 kg at sea level [29]. The CH-53K will initiate the catch phase at an altitude of 1.2 km altitude. An *International Standard Atmosphere (ISA)* model is used to determine that the helicopter can generate the amount of lift required to perform the catch at 1.2 km altitude [12].

When the helicopter is aligned in front and above the VuAB and the velocity vectors are matched, the coupling manoeuvre is
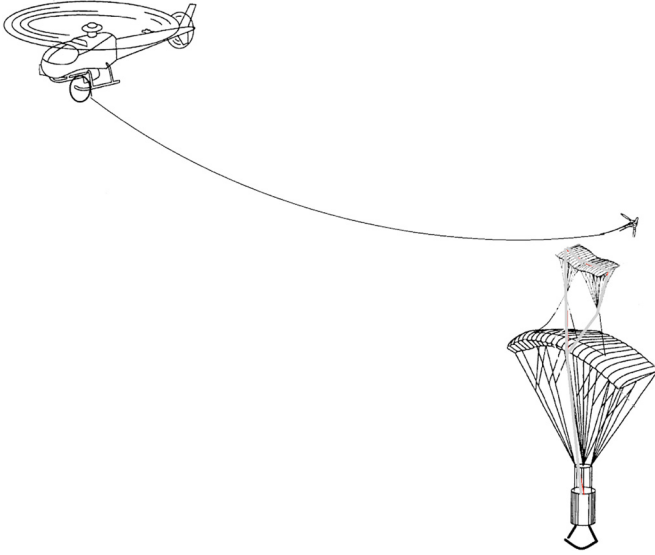
Fig. 12. An overview of the catch mechanism using a tandem parafoil configuration.

Table 6
Initial Pendulum Conditions for the 8-state helicopter model after catch in Section 7.

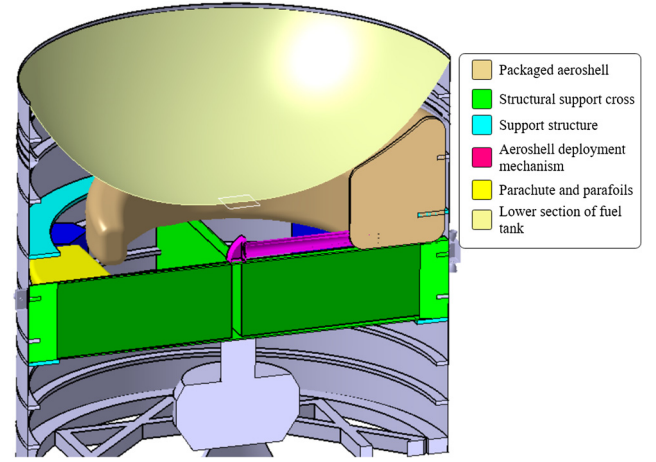|	θ_0 (rad)	$\dot{\theta}_0$ (rad/s)	$\ddot{\theta}_0$ (rad/s^2)
Lateral	0.009	0.018	0
Longitudinal	-0.49	-0.030	0

Fig. 13. Cross-section of the VuAB with folded aeroshell and parachute. (For interpretation of the colours in the figure(s), the reader is referred to the web version of this article.)

initiated. This attachment is performed using a non-clamping hook that is suspended from a cable and stabilised with a drogue basket. At the moment of catching, the cable allows a horizontal distance of 2 rotor diameters between the VuAB and the helicopter to mitigate the effects of helicopter down wash on the parafoil and catch mechanism. The hook attaches to a secondary parafoil on top of the main parafoil, aligned with the leading edge of the latter, as can be seen in Fig. 12. The secondary parafoil carries the load carrying cable that is attached to the VuAB.

To minimise the catching loads on the helicopter during catch, an attenuation device is used allowing a controlled 8 m expansion of the catching cable on the moment of contact with the secondary parafoil. A conservative mass estimation of the catch mechanism mounted on the helicopter is made based on reference data [23], resulting in a total mass of 738.8 kg. This includes the entire hoist system: a drum assembly, reeving system, hydraulic lines, valves, electric system components, helicopter drogue line and drogue parachute. The attenuation [23] reduces the maximum catch load on the helicopter from 180 kN to 123 kN which is within the helicopters envelope [20]. After the hook is locked on, the ΔV between the VuAB and helicopter is attenuated, after which the cable is reeled until the point of attachment is reached, leaving a line length of 42.21 m between the helicopter and the VuAB. Upon this process the main parafoil is discarded as the flight dynamics of towing the VuAB and the main parafoil are unstable.

To ensure stable helicopter flight after catch, rotational rates, velocities and Euler angles of the helicopter and VuAB combination are modelled using an 8-state 3D pendulum model. For safe operation, it is important that the system demonstrates stability upon load introduction for the catch, to prevent the pilots from having to perform too difficult manoeuvres. To assess this performance, simulations based on [14] are performed using the initial conditions given in Table 6. The simulations indicate that for zero pilot input, the system is stable in roll, but shows strong instability around the pitch axis, leading to diverging pitch angles as well as velocity. A constant control surface deflection upon catch is capable of opposing this. It is however advisable to use an automated controller for increased safety, and additionally to dampen out the slight oscillations around the pitch angles.

8. Configuration

The total recovery system mass amounts to 2789 kg, which is to be added to the first stage of the Ariane 6. Internal sources at

Airbus indicated that the payload penalty to GTO would realistically be around 0.25 kilograms for each added kilogram of first stage mass for Ariane 6. Therefore, the modifications will induce a payload penalty of 720 kg or 16% and 6% of the Ariane 62 and 64 GTO payload capacity respectively [18]. The recovery system packaging is visualised in the cross-section of the VuAB in Fig. 13. The Vulcain 2.1 engine is mounted below the green structural cross. The fuel pipes avoid the cross and do not interfere with the folded deployment mechanism.

Four attitude thruster clusters, each containing 4 thrusters in the same plane are mounted on the outside of the launcher at the height of the structural cross. These clusters are placed at an angle of 90° with respect to each other, to facilitate integration with the VuAB.

The parachute is placed opposite to the centre of the folded aeroshell to minimise the asymmetric mass shift due to the recovery system. The aeroshell folding pattern is determined using an assumed minimum folding radius of 152 mm based on a ablator thickness of 38 mm and a thickness of 20 mm for the supporting inflatable toroids [9]. The top of the folded aeroshell has a vertical margin of 100 mm with respect to the bottom of the propellant tank whereas the bottom of the folded aeroshell rests on the structural cross. The deflated aeroshell follows an accordion folding pattern. To fit inside the VuAB, these layers are wrapped around the longitudinal axis of the launcher. The centre of the aeroshell is mounted to the aeroshell deployment mechanism and located at a radius of 2100 mm from the centre in folded position. This leads to a shift of the *Centre of Gravity (CG)* of the launcher of 57 mm perpendicular to the longitudinal axis.

9. Discussion

This section elaborates on the significance of the work as well as on the limitations of the design. Firstly, a key design principle is to make use of systems with a TRL level that will allow development time within 4 years. Hence all components of the VuAB recovery system have a TRL of 5 to 7. It implies that the technology of those components has been demonstrated and system development is underway [32]. This is important for the operational

feasibility of the concept. The Ariane 6, for example, is planned to have the maiden flight late 2020, which is earlier than the moment that the recovery system could be operational after the needed development time. The integration of the recovery system is designed such that it requires minimal structural changes for the existing launcher, only requiring minor adjustments in the attachment points of the structural frame. This means that development, testing and integration of the recovery system can be done without necessary invasive measures into the development, production and operations process of the Ariane 6.

The current design is very sensitive to separation velocity. In case of using one boat and one helicopter for the final mid-air catch and landing, the allowable deviation from nominal separation velocity is 0.6%. This is a critical and possibly limiting parameter in the feasibility of the design. Currently, the Vulcain 2.1 engine is not re-ignitable. This is a major driver for the concept that is developed. Following current launcher developments, it is expected that a majority of future generation launchers have the possibility of re-ignitable engines. This will open up many different design options, such as the well-known booster landing. However, it would also allow for a significantly lower restriction on the deviation of separation velocity.

Lastly, a significant result is the low payload penalty of 720 kg. This is low compared to the payload capacity of the Ariane 6, especially considering the fact that the most expensive component can be refurbished and re-used. To assess the cost reduction, a cost breakdown was created that assessed the cost per launch for various scenarios. This is done using a parametric top down approach using the Transcost model by Dietrich Koelle [17]. This strategy was employed due to the lack of accurate component level cost data for a bottom up approach. With this model, the development cost, operational costs and production costs were estimated. These were subsequently used to determine the average costs per launch for various scenarios in the lifetime of Ariane 6. This analysis incorporated a learning factor on the production costs, while the number of launches per year and the number of times an engine can be reused were varied in these scenarios to evaluate the sensitivity to these parameters. These indicated that for a conservative scenario of 10 launches per year over the course of 20 years and 4 reuses for each engine, the average cost reduction per launch is expected to be 15%.

10. Conclusions and recommendations

The design of the first stage heavy launch vehicle recovery system facilitates separation of the VuAB and first stage, deployment and discarding of the aeroshell and parachute, deployment of the parafoil, and allows a helicopter to catch the VuAB and land it safely on a vessel. At launch, the recovery system will weigh 2789 kg with a payload penalty of 720 kg. The system can be integrated into the existing design of the launcher and will not interfere with nominal operations of the launcher. Implementing the recovery system can reduce the cost per launch of an Ariane 6 by 15%. Hence, both technical- and economic feasibility are demonstrated for the VuAB recovery system. Given the TRL of 5-7, a development time of 4 years maximum should be possible, allowing for a quick adaptation of the system.

Additional improvements on the VuAB recovery system design can be realized through further investigation of every part of the design due to the nature of conceptual design. Further work on the following considerations is recommended:

- A more accurate heat flux model during re-entry could indicate that it is possible to use an insulator instead of an ablator, which would reduce the aeroshell mass by 30%. This can in-

crease the re-usability and sustainability of the VuAB recovery system.
- A more detailed stability and controllability assessment can determine whether any (active) control elements are required during the reentry and aeroshell discarding.
- The current parachute and parafoil materials do not allow reuse after contact with ocean water. Improvements made to these materials could allow for re-usability which could reduce the overall costs and increase the sustainability of the VuAB recovery system.
- The packaging configuration causes a CG offset of 57 mm perpendicular to the longitudinal axis of the launcher, which has to be compensated by a counterweight. Optimisation of the packaging configuration might reduce this CG offset, removing the need of a counterweight.
- Increasing the space inside VuAB by changing the design of the liquid helium tank or the structural cross would allow the aeroshell, parachute, and parafoil to be packaged differently, reducing the complexity in structural attachments and deployment mechanisms.
- Re-ignition of the Vulcain 2.1 or a similar engine such as Prometheus [11] would allow control of the VuAB after separation and opens up a new array of design options that were discarded in earlier stages of the current design process. The VuAB could land on land, for instance by already giving a thrust boost in space.

Declaration of competing interest

None.

Acknowledgements

References

[1] A reusable Ariane thanks to Adeline, https://en.oclifescience.com/1554118-a-reusable-ariane-thanks-to-adeline. (Accessed January 2019).

[2] SpaceX Falcon 9 v1.2 data sheet, NASA, https://sma.nasa.gov/LaunchVehicle/assets/spacex-falcon-9-v1.2-data-sheet.pdf. (Accessed January 2019).

[3] National Aeronautics and Space Administration, Orion's parachute system, Retrieved from https://www.nasa.gov/sites/default/files/atoms/files/orion_parachutes.pdf, 2016.

[4] J.D. Anderson, Fundamentals of Aerodynamics, McGraw Hill Education Europe, New York, ISBN 978-0-07-339810-5, 2017.

[5] S. Dunker, J. Huisken, D. Montague, J. Barber, Guided Parafoil High Altitude Research (GPHAR) Flight at 57,122 ft, Airborne Systems, Pennsauken, Retrieved from https://arc.aiaa.org/doi/abs/10.2514/6.2015-2121, 2015.

[6] Patrick Blau, Ariane 5 - VA226 launch profile, spaceflight101, http://spaceflight101.com/ariane-5-va226/ariane-5-va226-launch-profile/. (Accessed 19 May 2019).

[7] Martin R. Cacan, Mark Costello, Michael Ward, Edward Scheuermann, Michael Shurtliff, Human-in-the-loop control of guided airdrop systems, Aerosp. Sci. Technol. 84 (2019) 1141–1149, https://doi.org/10.1016/j.ast.2018.08.008.

[8] D.K. Litton, D.M. Bose, F.M. Cheatwood, S. Hughes, H.S. Wright, M.C. Lindell, S.D. Derry, Inflatable Re-entry Vehicle Experiment (IRVE)-4 Overview, National Aeronautics and Space Administration, Washington, 2010, Retrieved from https://ntrs.nasa.gov/archive/nasa/casi.ntrs.nasa.gov/20110012170.pdf.

[9] Alicia M. Dwyer Cianciolo, Nasa Technical Reports Server (NTRS) - basic search, NASA, https://ntrs.nasa.gov/archive/nasa/casi.ntrs.nasa.gov/20100026676.pdf. (Accessed 18 January 2018).

[10] H. Wright, A. Cutright, J. Corliss, W. Bruce, D. Trombetta, A.R. Mazaheri, M. Coleman, A. Olds, S. Hancock, HEART Flight Test Overview, National Aeronautics and Space Administration, Washington, 2012, Retrieved from https://websites.isae-supaero.fr/IMG/pdf/137-heart-ippw-9_v04-tpsas.pdf.

[11] A. Iannetti, N. Girard, D. Tchou-Kien, C. Bonhomme, N. Ravier, E. Edeline, Prometheus, a LOX/LCH4 reusable rocket engine, https://doi.org/10.13009/EUCASS2017-537, 2017.

[12] ISO International Standard 2533-1975 "Standard Atmosphere First Edition", Corrigendum 1, ISO, Geneva, Switzerland, 1978.

[13] Justin Barber, Jean-Christophe Berland, Bill Gargano, Autonomous precision delivery of 42,000 pounds (19,000 kg) under one parachute, in: 20th AIAA Aerodynamic Decelerator Systems Technology Conference and Seminar, 2009, https://doi.org/10.2514/6.2009-2928.

[14] Honglei Ji, Renliang Chen, Pan Li, Real-time simulation model for helicopter flight task analysis in turbulent atmospheric environment, Aerosp. Sci. Technol. 92 (2019) 289–299, https://doi.org/10.1016/j.ast.2019.05.066.

[15] D. Lichodziejewski, A.P. Taylor, R. Sinclair, R. Olmstead, C. Kelley, J. Johnson, Development and testing of the orion CEV parachute assembly system (CPAS), in: AIAA Aerodynamic Decelerator Systems Technology Conference and Seminar, vol. 20, 2009, AIAA 2009-2938, Retrieved from https://ntrs.nasa.gov/archive/nasa/casi.ntrs.nasa.gov/20090015952.pdf.

[16] E.G. Ewing, H.W. Bixby, T.W. Knacke, Irvin Industries Inc. California Division and Air Force Flight Dynamics Laboratory (U.S.), Recovery System Design Guide, [Department of Defense], Department of the Air Force, Systems Command, Air Force Wright Aeronautical Laboratories, Air Force Flight Dynamics Laboratory, Recovery System Design Guide series, vol. 46, nr. 2, 1978.

[17] D.E. Koelle, Space launch systems cost estimation as design tool, Acta Astronaut. 34 (1994), https://doi.org/10.1016/0094-5765(94)90255-0, Retrieved from https://www.researchgate.net/publication/245139175_Space_launch_systems_cost_estimation_as_design_tool.

[18] Roland Lagier, Ariane 6 user's manual, Technical Report Issue 1, revision 0, ArianeGroup, Mar 2018, https://www.arianespace.com/wp-content/uploads/2018/04/Mua-6_Issue-1_Revision-0_March-2018.pdf.

[19] J.E. Johnson, R.P. Starkey, M.J. Lewis, Aerodynamic stability of re-entry heat shield shapes for a crew exploration vehicle, J. Spacecr. Rockets 43 (4) (2006) 721–730, https://doi.org/10.2514/1.20044.

[20] Lockheed Martin, CH-53K Sikorsky King Stallion Helicopter, Lockheed Martin, Bethesda, 2016, Retrieved from https://lockheedmartin.com/content/dam/lockheed/data/ms2/photo/Sikorsky/C-53K/Sikorsky-CH53K-SellSheet-English.pdf.

[21] Jeremie B.E. Meurisse, Jean Lachaud, Francesco Panerai, Chun Tang, Nagi N. Mansour, Multidimensional material response simulations of a full-scale tiled ablative heatshield, Aerosp. Sci. Technol. 76 (2018) 497–511, https://doi.org/10.1016/j.ast.2018.01.013.

[22] M. Naeije, W. Simons, E. Mooij, Ballistic Flight over the Earth, Part 1, Lecture Notes AE4870A Rocket Motion, Fac. Aerosp. Engin., TU Delft, 2017.

[23] R.V. Patterson, F.J. Fisch, H.D. Heyck, R.L. Jarvis, B.W. Mouring, 40,000-pound-capacity heavy-lift helicopter external load handling system design study, USAAVLABS Technical Report 68-16, U.S. Army Aviation Materiel Laboratories, Fort Eustis, Virginia, 1968, Contract DA44-l77-AMC-468(T), April 1968, Retrieved from http://www.dtic.mil/dtic/tr/fulltext/u2/671674.pdf.

[24] M. Rivier, J. Lachaud, P.M. Congedo, Ablative thermal protection system under uncertainties including pyrolysis gas composition, Aerosp. Sci. Technol. 84 (2019) 1059–1069, https://doi.org/10.1016/j.ast.2018.11.048.

[25] J.A. Samareh, Estimating Mass of Inflatable Aerodynamic Decelerators Using Dimensionless Parameters, National Aeronautics and Space Administration, Washington, 2015, Retrieved from https://ntrs.nasa.gov/archive/nasa/casi.ntrs.nasa.gov/20110014351.pdf.

[26] R. Winski, D. Bose, D.R. Komar, J. Samareh, Mission Applications of a HIAD for the Mars Southern Highlands, National Aeronautics and Space Administration, Washington, 2012, Retrieved from https://ntrs.nasa.gov/archive/nasa/casi.ntrs.nasa.gov/20130011614.pdf.

[27] M. Ward, M. Costello, N. Slegers, On the benefits of in-flight system identification for autonomous airdrop systems, J. Guid. Control Dyn. 33 (2010) 5, https://doi.org/10.2514/1.49030, Retrieved from https://arc.aiaa.org/doi/abs/10.2514/1.49030.

[28] MOOG Space and Defence Group, Moog propulsion | bipropellant thrusters, https://www.moog.com/content/dam/moog/literature/Space_Defense/spaceliterature/propulsion/bipropellant_thrusters_rev_0418.pdf. (Accessed 19 May 2019).

[29] W.R. Sturgeon, A Mathematical Model of the CH-53 Helicopter, National Aeronautics and Space Administration, Washington, 1980, Retrieved from https://ntrs.nasa.gov/archive/nasa/casi.ntrs.nasa.gov/19810003557.pdf.

[30] B.E. Tweddle, Simulation and Control of Guided Ram Air Parafoils, University of Waterloo report for course ECE 499, Department of Electrical and Computer Engineering, Waterloo, Canada, 2006, Retrieved from https://waterloouav.files.wordpress.com/2010/01/parachute.pdf.

[31] C. Toglia, M. Vendittelli, Modelling and motion analysis of autonomous paragliders, Retrieved from http://ojs.uniroma1.it/index.php/DIS_TechnicalReports/article/view/8850/8821, 2008.

[32] J.R. Wertz, D.F. Everett, J.J. Puschell, Space Mission Engineering: The New SMAD, Space Technology Library, Microcosm Press, ISBN 978-1881883159, 2011.

[33] A.M.D. Cianciolo, J.L. Davis, D.R. Komar, M.M. Munk, J.A. Samareh, J.A. Williams-Byrd, T.A. Zang, Entry, Descent and Landing Systems Analysis Study: Phase 1 Report, National Aeronautics and Space Administration, Washington, 2010, Retrieved from https://ntrs.nasa.gov/archive/nasa/casi.ntrs.nasa.gov/20100026676.pdf.